Dynamics behavior of flat glass panels under impact conditions: Experiments and numerical modeling

Satish Chaparala (SID Member)
Liang Xue
Da Yu
Seungbae Park

***Abstract* —** Response of brittle plate-like structures such as glass panels to impact loads has been the subject of many research studies. Different compositions of glass are used in wide variety of applications in daily life. Of interest in this study are the glass panels that are used in consumer electronics devices such as mobile phones, tablets, and televisions that help to protect the displays from every day wear and tear. Therefore, the requirement of this glass to resist scratches, drop impacts, and bumps from everyday use leads to the importance of investigation of the glass response under dynamic impact loading. Ball drop test is a widely accepted test for impact reliability in the industry. The test specifies the impact energy threshold as a qualification and prediction metric. Use of energy as the key parameter in impact testing is limited, because it does not account for the time spent in contact during the impact event. This study attempts to establish a reliable metric for impact testing based on a momentum change. The deformation and the strain of the glass will be obtained by the digital image correlation system, while the rebound velocity will be measured with the high-speed cameras. The global and local measurements are conducted to verify the accuracy of the experimental results. Finite element analysis is conducted using ABAQUS to provide a comprehensive understanding of the dynamic response of the glass. Constitutive relationship for a tape, a hyperelastic material, is developed in this study. Good correlation in deflection time history is obtained between the measurements and predictions.

Keywords *— strengthened cover glass, ball drop, digital image correlation, finite element analysis.*
DOI # 10.1002/jsid.283

1 Introduction

As the demand for touch screen technology increases, there has been a growing interest, particularly in last few years, in the resistance of cover glass to impact loads. Typically, the applications demand harder, stronger, yet thinner glass that resists scratches and survives in drop impacts. The glass could be subjected to impact loads during manufacturing, shipping and field use, maintenance, and so on. Consequently, the impact behavior of glass under impact loading is an important phenomenon to be investigated. Similar studies have been carried out in the past by several researchers.[1–10] However, most of the results presented in the literature are related to the laminated glass structure or for a very thick glass. The current applications of interest are primarily focused on single thin layer of glass (less than or equal to 0.7 mm). The first principal strain results and the influence of the momentum change are not discussed in the prior studies reported.

The objective of this study is to investigate the dynamic analysis of glass under ball drop impact. Experiments are performed using digital image correlation (DIC) to measure the deformation and strain of glass panel under ball impact. Finite element analysis using commercially available finite element code, ABAQUS, is carried out, and the predicted behavior of the glass panel is compared with that of the measured in terms of deflection and strains. The effect of the magnitude of the impact energy, size of the ball used to impact the panel on the glass panel deflection, and first principal strain and momentum change are examined. Three different impact energies, 0.5, 1, and 2 J, and three steel balls size, 0.75, 1, and 2 in diameter are chosen. Some of the works reported in this draft are presented earlier at an International Technical Conference and Exhibition on Packaging and Integration of Electronic and Photonic Microsystems (InterPACK).[11] The constitutive relationship development of the hyperelastic material used in the experiments is further added to the current draft. In addition, results from the modified and improved numerical model are presented.

2 Experiments

In this section, DIC technique and the associated experimental setup is described. DIC is a full-field optical measurement technique in which both the in-plane and out-of-plane deformations and strains are computed by comparing the images of the target object at initial and deformed stages (Fig. 1).[12] Thousands of unique correlation areas (known as subsets)

Received 10/15/14; accepted 02/24/15.
Satish Chaparala is with the Modeling and Simulation, Corning Incorporated, Corning, NY, USA; e-mail: ChaparalSC@corning.com
Liang Xue, Da Yu and Seungbae Park are with the Department of Mechanical Engineering, Binghamton University, Binghamton, NY, USA.

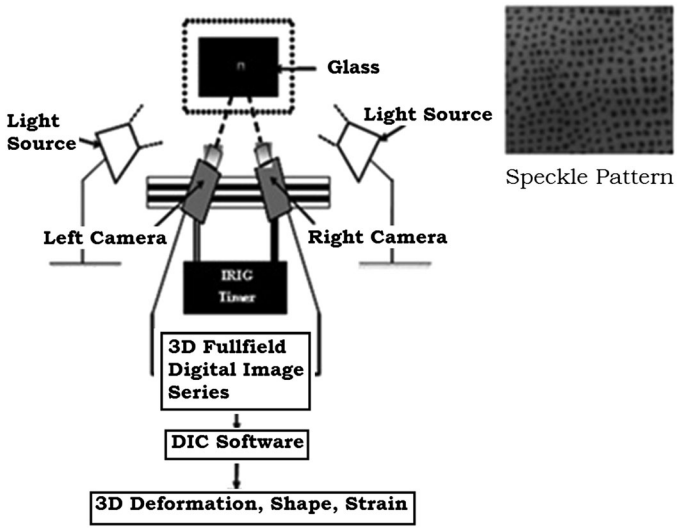

FIGURE 1 — High-speed digital image correlation.

are defined across the entire imaging area. These subset centers are tracked, in each successive pair of images, with accuracy of up to one hundredth of a pixel. Then, using the principles of photogrammetry, the coordinates of each facet are determined for each set of images. The results are the 3D surface profile of the component, the displacements, and the strains. Rigid body motion can first be quantified and then removed to reveal relative deformations.[7] There are several advantages of using this technique compared with the traditional strain gauge method. This technique provides the displacement profile of the entire glass panel. The strain gauge attachment process may lead to more flaw introduction in the panel and can compromise the strength of the panel. There could be size limitations on the strain gauges available, and therefore, it is not quite possible to obtain the accurate estimate of the strains in highly localized areas. This is feasible with DIC.

A glass panel of 950 mm × 590 mm × 0.7 mm is attached to a rigid aluminum frame on all four sides using a double-coated polyethylene foam tape. It is conformable closed cell foam with a high strength acrylic adhesive that provides good initial tack and offers high ultimate adhesion to a wide variety of surfaces. Figure 2 shows the details of the experimental setup. Fishing line and black tape are used to connect the steel ball to the pendulum swing tower. The weight effect from the fishing line and black tape is negligible compared with the weight of the steel ball. The pendulum swing can be manually adjusted to the desired length, thus controlling the drop height of the ball. The impact orientation is a critical factor affecting the impact responses of glass. To eliminate any initial perturbation when releasing the steel ball, a magnetic switch is applied to ensure the repeatability of impact orientation. The glass panel is mounted to the aluminum frame, which can be adjusted according to the glass panel size. High-speed digital cameras have been set up to capture pictures of the glass panel surface during impact frame by frame.

Six halogen lights provide the same light intensity for exposure time less than 10 μs. Pre-impact and Post-impact portions of the impact are extracted in the form of series of images. These images are then exported to post-processing software, ARAMIS (Braunschweig, Germany),[13] to solve for the full-field deformations, 3D profile, and the strain of glass panel. Five experiments are conducted for different steel balls sizes and impact energies. Each experiment is repeated five times with same sample. All the five experiments and the values of the impact velocity depending on the ball size and energy are presented in Table 1. The impact velocities shown in the table are calculated using $v = \sqrt{2E/m}$.

3 Results and analysis

3.1 Potential energy versus the glass deflection

First, the glass panel is impacted with 2-in.-diameter steel ball from different heights resulting in the impact energy of 0.5, 1,

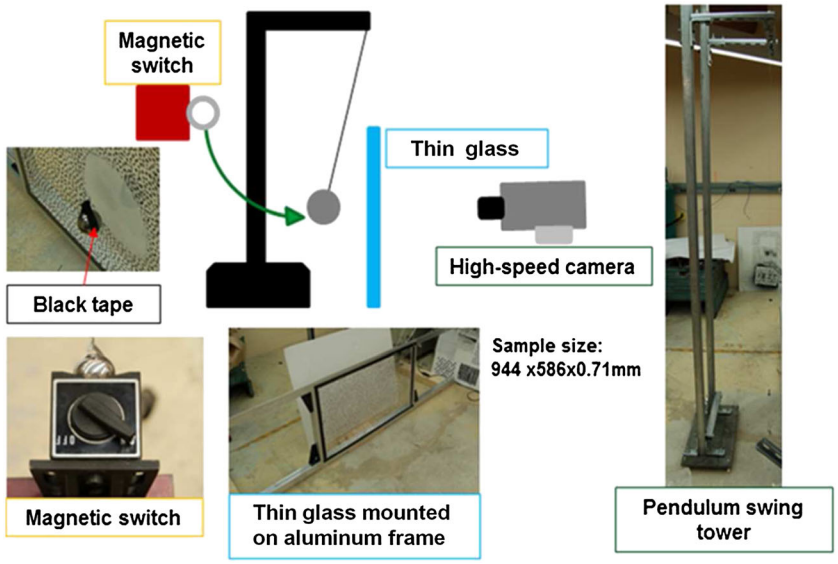

FIGURE 2 — Glass impact test setup.

TABLE 1 — Five cases studied with different ball size and impact energy.

Ball size (in.)	Ball mass (g)	Energy (J)	Impact velocity (m/s)
0.75	28.2	0.5	5.953
1	66.8	0.5	3.867
2	535	0.5	1.367
2	535	1	1.933
2	535	2	2.734

1.5, and 2 J. Figure 3 shows the global deflection of the panel at three different time instants. As expected, the maximum deflection of the glass panel increases with the increase in the potential energy. Figure 4 shows the line plot of the time history of the deflection of the glass panel.

Next, the glass deflection is measured when impacted with different ball diameters (0.75, 1, and 2 in.) from different heights, maintaining the same potential energy of 0.5 J. It can be observed from Figure 5 that the different ball sizes resulted in different deflection in spite of maintaining the same potential energy. This is due to the different interactions of the ball with the panel during the impact. The values shown are the average of three repeats of each experiment. For instance, the 2-in. ball deforms the glass 141% more than the 0.75-in. ball. The glass panel conforms to the ball shape locally in the case of 2-in. ball whereas it does not happen with smaller diameter balls (0.75 and 1 in.). Therefore, it is quite apparent that the "energy", as a parameter for impact qualification and failure metrics, may not be appropriate. It should

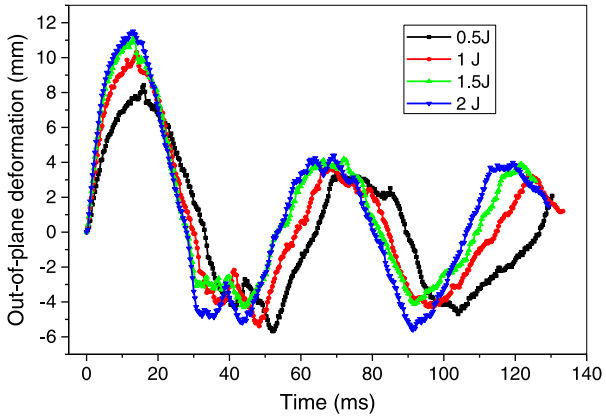

FIGURE 4 — Out-of-plane deformation responses of 2-in. ball at different potential energy for 40-in. glass.

be replaced with a parameter that can result in a relationship with the glass deflection that accounts for the ball geometrical profile and the time spent in contact with the target surface. This paper proposes momentum change as such a parameter. The rebound velocity must be extracted from experimental results to establish momentum change.

3.2 Rebound test

The rebound test is performed to obtain the impact velocity and rebound velocity of steel balls with different sizes to calculate the energy loss and the momentum change during

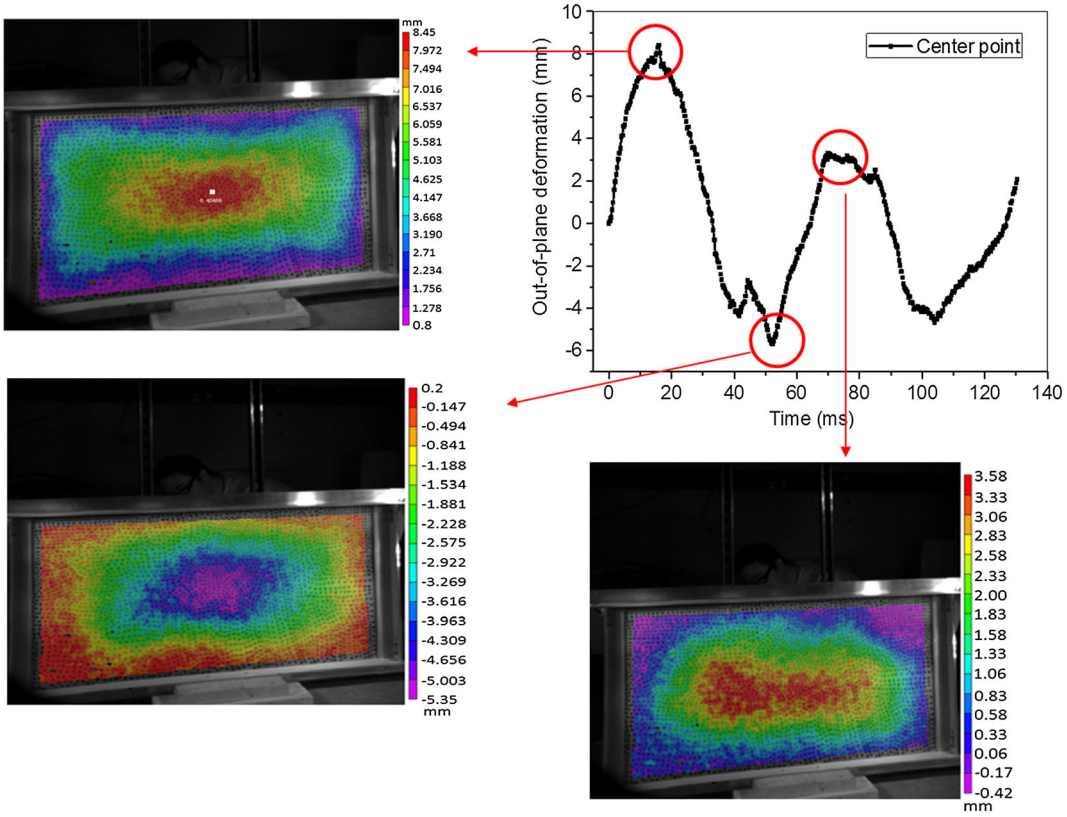

FIGURE 3 — Global deformation of 2-in. ball at 0.5 J for 40-in. glass.

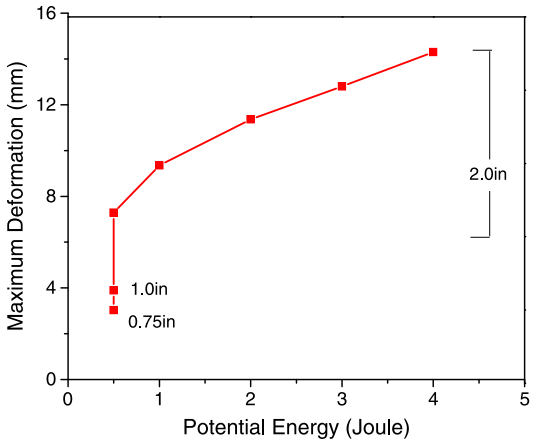

FIGURE 5 — Nonlinear relationship between the maximum deformation and the drop energy.

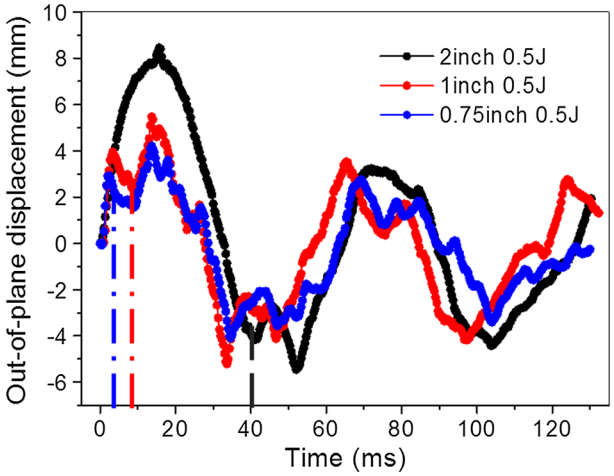

FIGURE 7 — Effect of impact ball size.

the impact event. The energy loss is calculated as $E_{loss} = \frac{mv_{impact}^2}{2} - \frac{mv_{rebound}^2}{2}$. The momentum change is calculated as "$m(v_{impact} - v_{rebound})$". In the rebound test (potential energy range of 0.5–4 J), one high-speed camera (Photron Fastcam APX Rs) is placed perpendicular to the side of the sample glass with the frame rate set at 10,000 fps (Fig. 6). The experimental velocity is calculated by comparing pictures taken by the high-speed camera. The relative distance traveled by the ball center between sequential frames is averaged over three trials of ball drops for each test case.

The measured impact velocity is slightly smaller than the calculated impact velocity due to friction. According to the rebound test, the steel ball detaches from the glass panel after 4, 8, and 40 ms for 0.75-in., 1-in., and 2-in. steel ball, respectively (Fig. 7). As the steel ball size increases, the momentum change for steel ball increases, which explains the longer time for the large size steel ball to detach from the glass panel after impact. Figure 8 shows the deflection map of the glass panel (at the impact location) when impacted with different ball diameters. The larger steel ball leads to higher glass deformation due to the higher momentum change (Table 2). It is interesting to notice that there is spatial oscillation of glass panel around the impact point when it is impacted with small ball.

It is clearly shown that the maximum out-of-plane deformation is related to momentum change of impact ball rather than its initial potential energy. The deformation of the glass depends on a combination of factors: the ball diameter and velocity, as well as the contact response of the glass. With this relation, one could reasonably predict maximum deformation results for other cases. The relation is linear because the momentum change is directly related to the impulse force that is transferred to flex the glass to the point of maximum deflection. There are some momentum transferred to cause oscillations in the glass plate; thus, the deformation to momentum ratio does not pass through the origin. Once the deformation of glass panel is estimated, maximum momentum change can be obtained from the relationship developed in this study (plot shown in Fig. 9). The momentum change value estimated can then be used to compare different test conditions. This is a better metric to compare different test conditions as opposed to the kinetic energy.

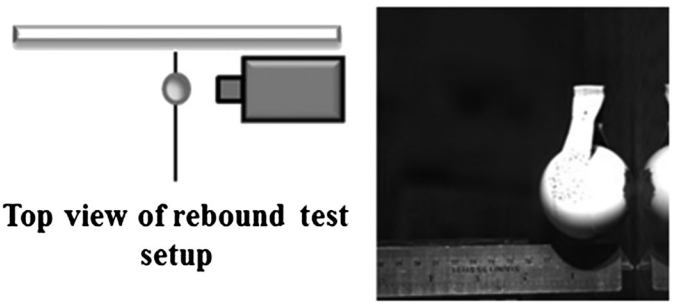

FIGURE 6 — Rebound test setup.

3.3 Digital image correlation global versus local measurement

The frame rate of global measurement is only 3000 fps, which means only 3000 pictures are captured during 1 s. In order to obtain more detailed information of the dynamic response at impact area, local measurement with 30,000 fps is applied to record the impact event. Figure 10 shows the comparison of the deflection response obtained from global and local measurements. There is not much difference in the first peak of the deflection. The latter time history shows some small differences.

3.4 Strain measurement

The DIC software has a built-in algorithm to compute the strain field. Only the in-plane strains in the 11 and 22 directions are computed from the displacement field. The strain in the 33 (out-of-plane) direction is calculated by plane stress or plane strain models. Incompressibility of the solid body is assumed.[9] Figure 11 shows that the first peak of strain at impact point occurs earlier than that of out-of-plane

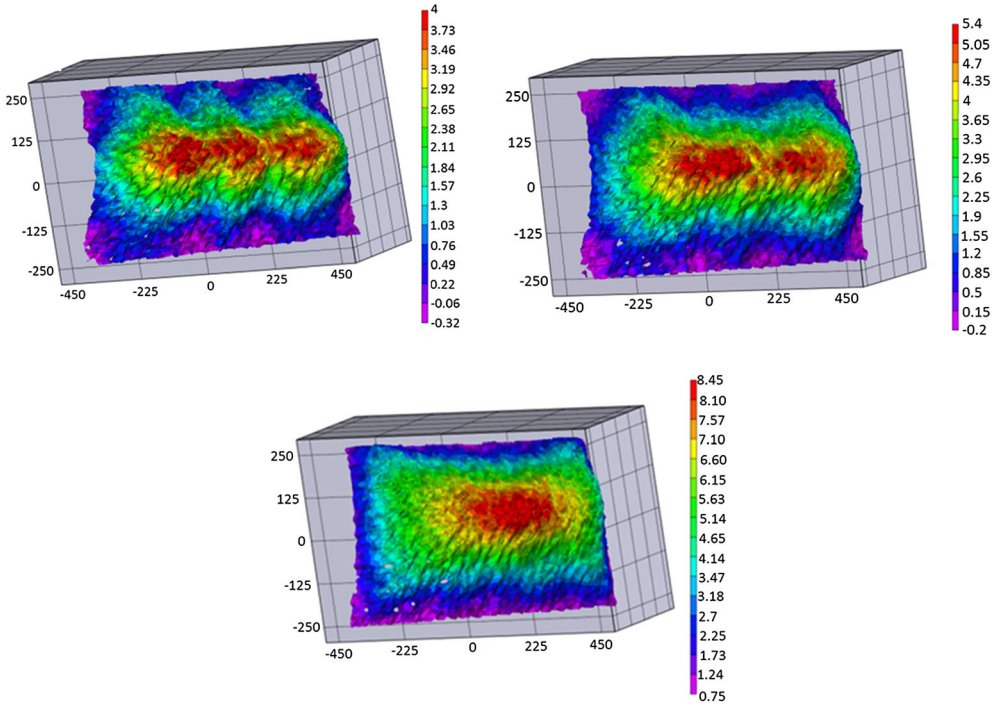

FIGURE 8 — Maximum out-of-plane deformation for impact ball of different size.

TABLE 2 — Rebound test results from experiment.

Theoretical energy	J	0.5	0.5	0.5	1	2	3	4
Impact ball diameter	in.	0.75	1	2	2	2	2	2
Calculated impact velocity	m/s	5.96	3.87	1.37	1.93	2.73	3.35	3.87
Experimental impact velocity	m/s	5.66	3.77	1.35	1.87	2.65	3.27	3.79
Experimental rebound velocity	m/s	0.98	0.68	0.65	0.81	1.00	1.15	1.24
Energy loss	J	0.44	0.46	0.38	0.76	1.61	2.51	3.42
Experimental momentum change	kg m/s	0.19	0.30	1.07	1.43	1.95	2.36	2.69

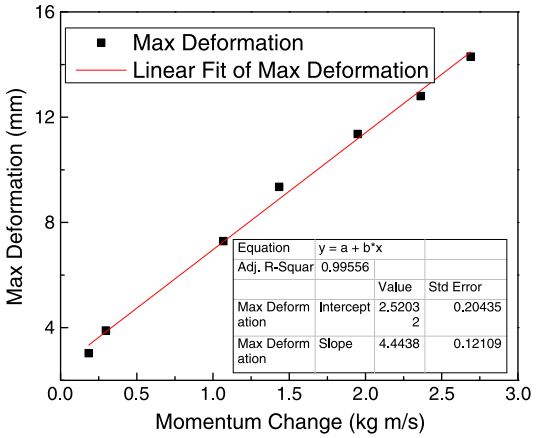

FIGURE 9 — Linear relationship between out-of-plane deformation and momentum change.

deformation. This is because the glass conforms to the ball as soon as it gets impacted, and therefore, the strain is high at that time instant. As the glass continues to bend globally, there are times instants when the ball loses the contact with the glass. As the glass vibrates structurally, it could impact the ball again. This leads to multiple peaks in the strain history. Smaller ball (1 in.) results in higher strain magnitude (leads to higher stress) compared with the large size ball (Fig. 12). This is because the contact area in the case of smaller balls decreases and the bending strain increases (because bending strain, $\epsilon = t/2\rho$, where "ρ" is the radius of curvature). The maximum strain developed in the panel depends on the local behavior of the panel, not the global deflection.

4 Finite element modeling

This section presents the finite element analysis, wherein the modeling aspects such as material properties, boundary conditions, loading, meshing, and effect of mesh density on the results and different modeling strategies are discussed. The predicted deflections and strains are compared with those of measured results discussed in previous sections. The dimensions of the cover glass are 950 mm × 590 mm × 0.7 mm. Finite element software that is commercially available, ABAQUS, version 6-13.2, is used in this study. The domain of the cover glass is discretized using continuum shell

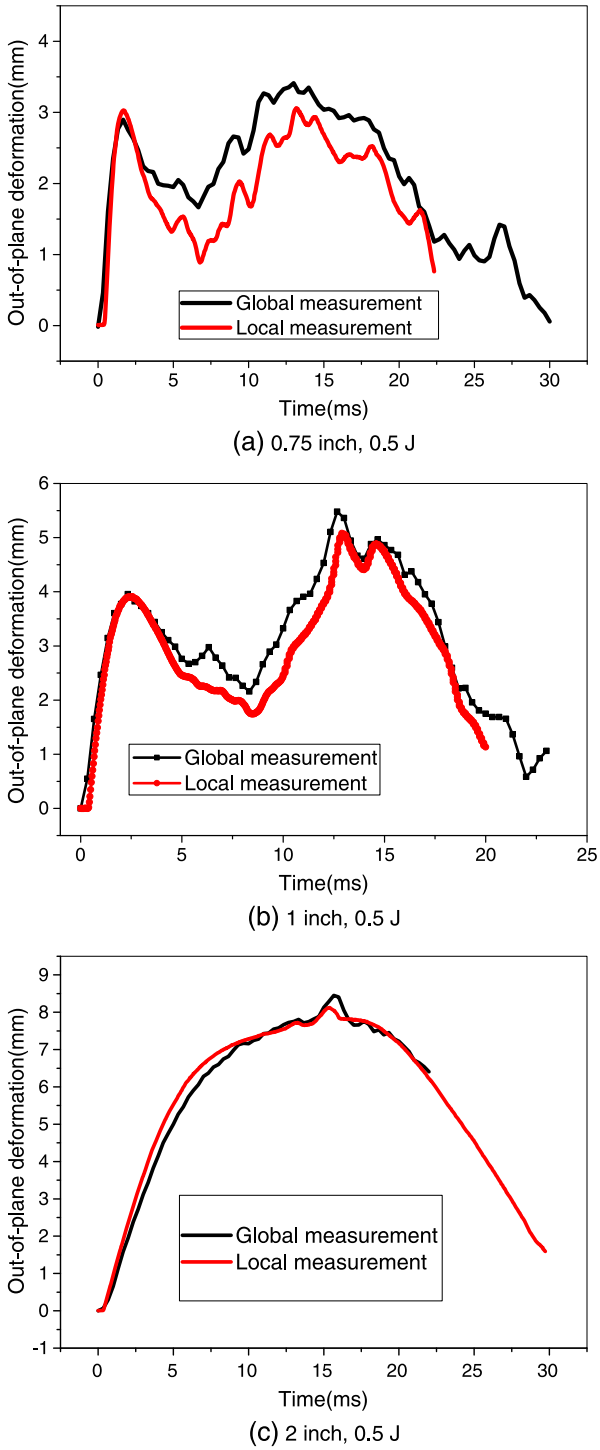

FIGURE 10 — Comparisons between global and local measurement of different size balls at 0.5 J.

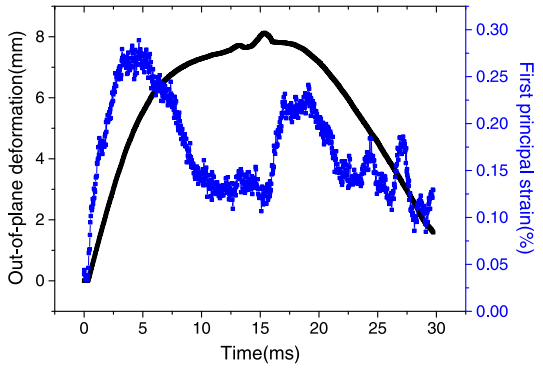

FIGURE 11 — Strain and deflection responses of 2-in. ball with 0.5 J.

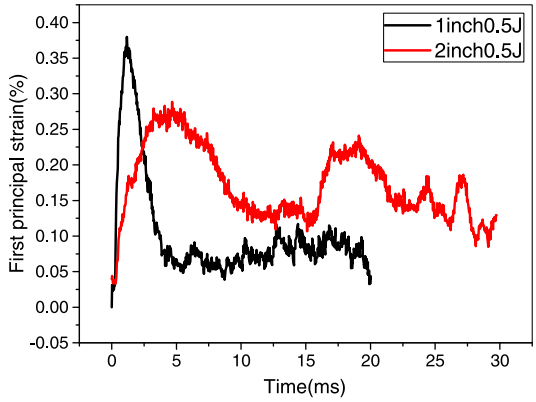

FIGURE 12 — Strain responses of impact ball with different size.

elements, identified as SC8R in ABAQUS, which stands for continuum shell with eight nodes and three translational degrees of freedom at each node. The shell element accounts for bending and membrane stresses. Reduced integration is used to evaluate the stiffness matrix (to avoid element locking). There is one element through the thickness of the plate (because this is a shell element). Simpson's rule is used for integration with five points through the thickness of the shell element. It is recommended to mesh the panel by dividing the panel into different regions and varying the element size in each region. The mesh density has to be fine in the regions of interest (which is the point of ball impact on the panel), and the density can be relaxed elsewhere. This strategy will optimize the total number of elements generated in the model and reduces the computational time.

Because this is a time-dependent problem, meshing plays a significant role in saving computational time. The ball is discretized using 3D tri-linear continuum solid element. This element is referred to in ABAQUS as C3D8R, which stands for 3D continuum solid element with eight nodes with three translational degrees of freedom at each node. Reduced integration is used to evaluate the stiffness matrix. The total time of analysis is divided into 600 points, and the output is requested at these time instants. The constitutive relation of glass and ball is linear and elastic. As discussed in previous sections, the glass panel is attached to the aluminum frame using a double-coated polyethylene foam tape. This material is characterized for its constitutive material behavior. Three different tests are conducted, namely, uniaxial tensile test, planar tension test, and compression tests.

Elastomeric material models are characterized by different forms of their strain energy density functions. Implicit in the use of these functions (usually denoted by W) is the assumption that the material is isotropic and elastic. The derivative

of W with respect to the strain results in the stress–force per unit area. The commonly available strain energy functions have been represented either as functions of strain invariants that are functions of the stretch ratios or directly in terms of the stretch ratios themselves. Strain is a measure of deformation (or geometric changes). In the case of hyperelastic materials, the stretch ratio, λ , is defined as the ratio of the deformed guage length, L, divided by the initial gauge length, L_o. If "e", be the engineering strain, $\lambda = 1 + e$ $\left(\lambda = \frac{L}{L_o} = \frac{L_o + L - L_o}{L_o} = 1 + \frac{L - L_o}{L_o} = 1 + e\right)$. Generally, if an in-plane biaxial load is applied to a piece of hyperelastic material, three principal stretch ratios in the three respective principal directions can be defined. In large deformation analysis of nonlinear materials (such as elastomers), the stretch ratios are a convenient measure of deformation and are used to define strain invariants, I_j, for j = 1; 2; 3 that are used in many strain energy functions. The three strain invariants can be expressed as follows:

$$I_1 = \lambda_1^2 + \lambda_2^2 + \lambda_3^2$$

$$I_1 = \lambda_1^2\lambda_2^2 + \lambda_2^2\lambda_3^2 + \lambda_3^2\lambda_1^2$$

$$I_3 = \lambda_1^2\lambda_2^2\lambda_3^2$$

In case of perfectly incompressible material, the third invariant is unity, $I_3 = 1$. The polynomial hyperelastic material model is a phenomenological model of rubber elasticity. In this model, the strain energy density function is of the form of a polynomial in the two invariants I_1 and I_2 of the left Cauchy–Green deformation tensor. The strain energy density function for the polynomial model is as follows[14]:

$$W = \sum_{i,j=0}^{n} C_{ij}(I_1 - 3)^j(I_2 - 3)^j$$

For compressible materials, a dependence of volume is added. In this study, the tape is modeled as incompressible material. The data obtained from three tests indicated earlier in the text are curve fitted into this model, and $n = 3$ is chosen. The following constants shown in Table 3 are obtained. Table 4 provides the material properties of glass and the stainless steel.

In the model, the ball is positioned such that it just touches the glass. Initial velocity is prescribed on all the nodes of the ball. The initial velocity is estimated from the corresponding drop height using $V = (2hg)$. A general contact condition is applied in the model. The contact interaction properties are "hard contact", "no penetration allowed" in the normal direction, and "no friction" in the tangential direction. Explicit analysis is used in this study. Following displacement and strain plots show the correlation between measurements and the predictions from the finite element analysis.

TABLE 3 — Constants in the constitutive model of the tape.

C10	C01	C20	C11	C02	C30	C21	C12	C03
0.376	−0.222	−0.12	0.214	−0.0846	−0.00136	0.0116	0.00177	−0.000117

TABLE 4 — Material properties of the glass and the steel ball.

Material	Elastic modulus (MPa)	Poisson ratio	Density (kg/m^3)
Glass panel used in this study	71,700	0.21	2440
Stainless steel	200,000	0.29	8000

The correlation between the predictions and measurements in deflection of the glass panel is excellent. It can be observed from Figure 13 that the time history of the deflection is accurately captured including the minor peaks and the time instants of their occurrence. There is one deflection peak in the glass panel when impacted with 2-in. ball. There are two peaks in case of 0.75-in. and 1-in. balls with second peak slightly higher than the first peak. This is because the glass panel structurally vibrates as it globally deflects. The structural wave reflects back and forth from the boundaries must faster when impacted with 0.75-in. and 1-in. ball. The finite element model is able to capture the time history of the glass panel deflection very accurately. Figure 14 shows that there are two peaks in the strains in the case of 2-in.-diameter ball whereas there is only one peak in the case of 1- in.- and 0.75-in.-diameter balls. In the case of 2-in.-diameter ball, once the ball impacts the panel, it travels with the glass panel as the glass panel deflects. During the travel, the glass loses its contact due to the structural waves setup in the panel. As the glass panel and ball continues their travel, the glass panel gets hit by the ball again resulting in the second peak. In case of 1 and 0.75 in., the balls rebound back with larger velocities and the glass panel deflects without any further interaction with the ball. So there is only one peak. The correlation between the predictions and measurements in strain needs further investigation. The magnitudes of the first principal strain predicted are higher than those of measurements (in one case 2X). The mass damping of the glass panel plays significant role in affecting the strain response. Figure 14(a) shows that the prediction without considering damping predicts higher second peak in the strain whereas the inclusion of damping results in the prediction that is consistent with that of measurement. The accurate value of damping needs to be investigated. The damping did not make any difference in the predicted strain responses in case of 1 and 0.75 in. ball cases. There is only one peak in the strain response in these two cases. The area of the maximum strain occurrence is very small. So the uncertainty in the strain measurement in this much localized area is being analyzed as well. The strain rate in the glass panel is calculated by dividing the maximum strain by the time taken to result in the maximum strain. This strain rate is significantly different between different ball sizes for the same impact energy. The highest strain rates are experienced by the glass hit with the smallest diameter ball. The strain rates, at equivalent energies, are as much as 11 times greater for a ball with a 0.75-in. diameter compared with a 2-in.-diameter ball. The strain rate is directly affected by the ball diameter, as the impact contact area is much smaller.

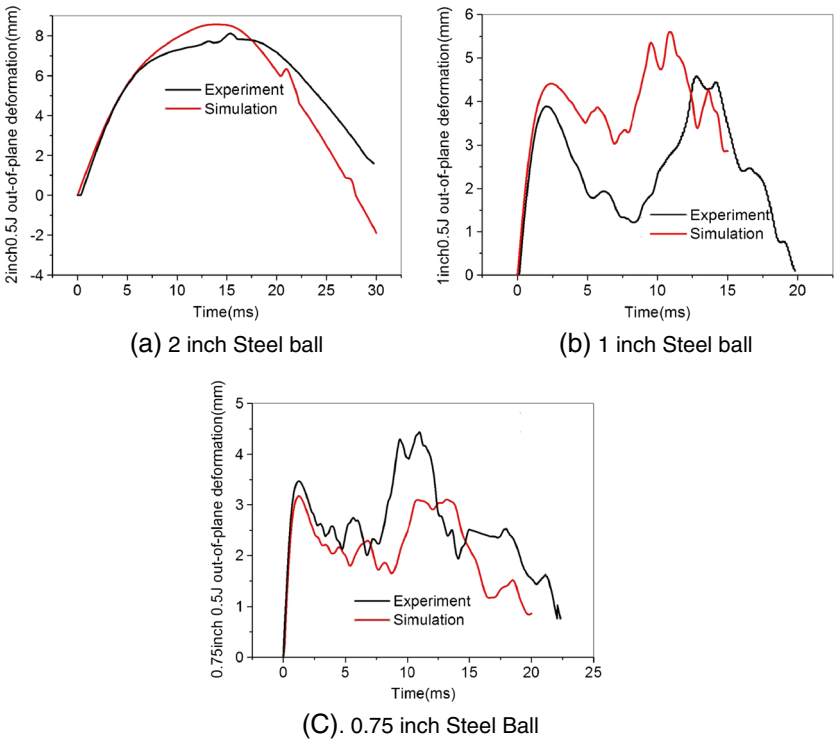

FIGURE 13 — Deflection response comparison between measurements and predictions (different ball sizes imparting same energy 0.5 J).

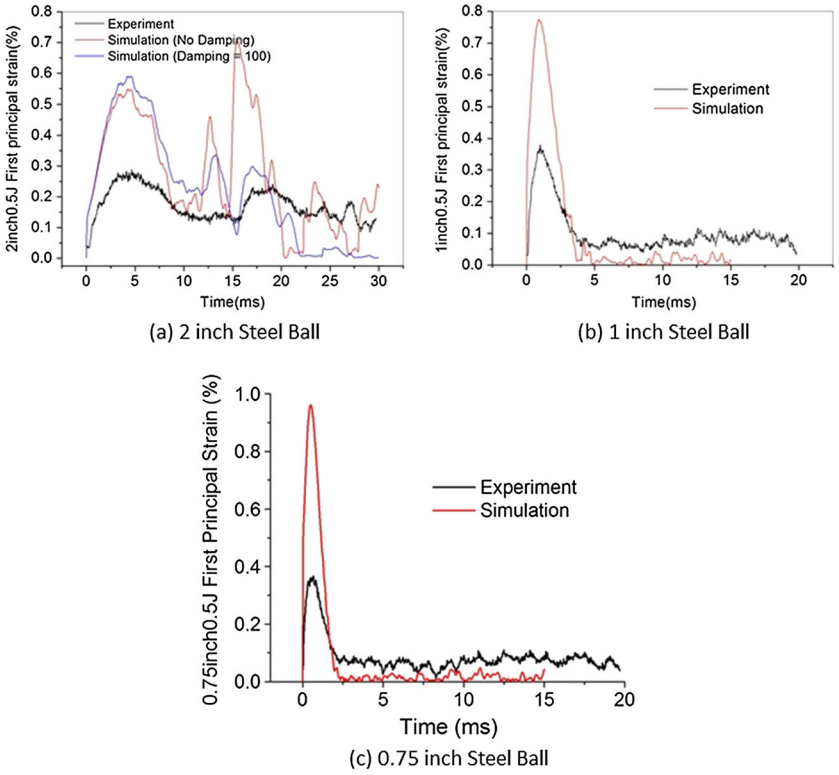

FIGURE 14 — Strain response comparison between measurements and predictions (different ball sizes imparting same energy 0.5 J).

5 Conclusions

The capability of DIC optical technique to measure deflection and strains of glass panel is demonstrated. Normally, a strain gauge is used to do this kind of analysis, and this new technique would provide additional advantages. The advantages are that this is a non-contact technique, and it has the ability to generate the complete map of the deflection and the strain of the glass panel and the ability to capture the dynamic impact response at a very high frequency. Also, high resolution over a small area is possible. Excellent correlation in maximum deflection was obtained between the measurements and predictions. Correlation in strain magnitudes vary in different cases. There is more noise for smaller ball, and the noise filter in the software reduces the strain value. Out-of-plane deformation is related to momentum change of impact ball rather than its initial potential energy. Momentum change is linearly related to the maximum deformation of the glass due to the transfer of momentum into the flexure of the glass. The momentum change accounts for the time spent in contact with the glass and the contact area. The larger the ball size, the greater the time spent in contacts with the glass, the larger the momentum change. An energy parameter does not account for the geometry of the ball and the time of the impact event. Momentum change is better suited to predict maximum deformation. The strain rate is inversely proportional to the ball diameter. The strain rate affects the glass vibrational response, resulting in high oscillations in the local impact area. The smaller strain rates, with the larger ball diameters, result in a lower frequency vibrational response. The time instant at which the maximum principal strain occurs is much earlier than the time instant at which the maximum deformation occurs. This is due to the maximum strain occurring locally due to the glass deflection conforming to the ball, while the maximum deformation is a result of a global momentum transfer.

References

1 J. L. Glathart and F. W. Preston, "The behavior of glass under impact: theoretical considerations," *Glass Technol.* **9**, No. 4, 89–100 (1968).
2 S. Bouzid *et al.*, "Fracture criterion for glass under impact loading," *Int. J. Impact Eng.* **25**, 831–845 (2001).
3 P. Kumar and A. Shukla, "Dynamic response of glass panels subjected to shock loading," *J. Non Cryst. Solids* **357**, 3917–3923 (2011).
4 S. W. Chung and J. W. Jeong, "Drop reliability of glass panel for LCD," IEEE Proceedings of Electronic Components Technology Conference, 2011.
5 A. Ball and H. W. McKenzje, "On the low velocity impact behavior of glass plates," *Journal De Physique IV, Colloque C8, Supplement au Journal de Physique III* **4**, 783–788 (1994).
6 N. R. Mathivanan and J. Jerald, "Experimental investigation of low-velocity impact characteristics of woven glass fiber epoxy matrix composite laminates of EP3 grade," *Mater. Des.* **31**, 4553–4560 (2010).
7 M. C. Pan *et al.*, "Drop simulation and experimental validation of TFT-LCD monitors," IEEE Proceedings of Electronic Packaging Technology Conference 269-274.
8 F. W. Flocker and L. R. Dharani, "Stresses in laminated glass subjected to low velocity impact," *Eng. Struct.* **19**, No. 10, 851–856 (1997).
9 D. Yu *et al.*, "Dynamic responses of PCB under product-level free drop impact," *Microelectron. Reliab.* **50**, 1028–1038 (2010).
10 S. B. Park *et al.*, "Measurement of transient dynamic response of circuit boards of a hand-held device during drop using 3D digital image correlation," *J. Electron. Packag.* **130**, No. 4, 0445021–0445023 (2008).
11 L. Xue *et al.*, "Dynamic analysis of thin glass under ball drop impact with new metrics," Proceedings of InterPACK, ASME Conference, San Francisco, CA, USA, July 16–18, 2013.
12 W N. Sharpe, "Handbook of Experimental Solid Mechanics," Society of Glass Technology: Sheffiled, South Yorkshire, UK, *pp* 565–599.
13 http://www.gom.com/3d-software/aramis-software.html
14 A. Bower, "Applied Mechanics of Solids," First Edition, CRC Press: Abingdon OX, 2009.

Dr. Chaparala joined Corning Incorporated as a Research Scientist Packaging in 2006. He was promoted to Sr. Research Scientist Packaging in 2010. He moved to core Modeling and Simulation group in 2014. His major areas of expertise are in the area of computational modeling of structural mechanics and heat transfer problems. He has four granted patents and four patent applications pending. He is the author/co-author of 1 book chapter, 12 Journal papers, and 22 conference publications. In the past, he is the recipient of Excellence in Research Award at Binghamton University in 2006, recipient of Journal of Electronic Packaging best paper of the year 2009 award, and co-author of a paper in Green Laser that won distinguished paper of the conference award. Dr. Chaparala also works as Adjunct Faculty in the Mechanical Engineering Department at SUNY Binghamton. He is the Associate Guest Editor of ASME Journal of Electronic Packaging and also serves on Executive Committee of the ASME Electronics and Photonics Packaging Division (EPPD). Dr. Chaparala obtained his MS and PhD in Mechanical Engineering from the State University of New York at Binghamton under Prof. Bahgat Sammakia in 2006.

Liang Xue received his bachelor's degree in Mechanical Engineering at Xi'an Jiaotong University in 2010. He joined as a PhD student in the Department of Mechanical Engineering at the State University of New York at Binghamton in 2010. His research interests are in the area of reliability assessment of electronic packages under drop/impact and thermal loading with numerical simulation (FEA) and experimental measurement.

Da Yu received his PhD from SUNY Binghamton University in 2012 in Mechanical Engineering. After graduation, Dr. Yu worked for Apple as a senior FEA engineer responsible for touch and display module. Dr. Yu has more than 17 technical publications and 1 US patent so far. His research interest is physics of reliability and finite element analysis for microelectronics packaging touch and display module.

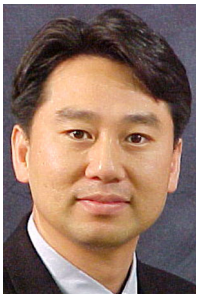

Seungbae Park received his PhD at Purdue University in 1994. Dr. Park worked for IBM as a development and the reliability engineer responsible for flip chip technology. Since 2002, Dr. Park is teaching at the State University of New York at Binghamton as a professor of mechanical Engineering department. He has more than 100 technical publications and 4 US patents. Dr. Park has been serving for many technical communities such as chairing iNEMI's Modeling & Simulation Technical Work Group, "Electronics Packaging" council in the Society of Experimental Mechanics, and reliability committee member of ECTC and ASME. Dr. Park's research interest is physical reliability for microelectronics and MEMS packaging.